APPENDIX F

Target Fragments in Collisions of 1.8 GeV/Nucleon ^{56}Fe Nuclei with Photoemulsion Nuclei, and the Cascade-Evaporation Model

by

V.E. Dudkin, E.E. Kovalev, N.A. Nefedov
V.A. Antonchik, S.D. Bogdanov, V.I. Ostroumov
E.V. Benton and H.J. Crawford
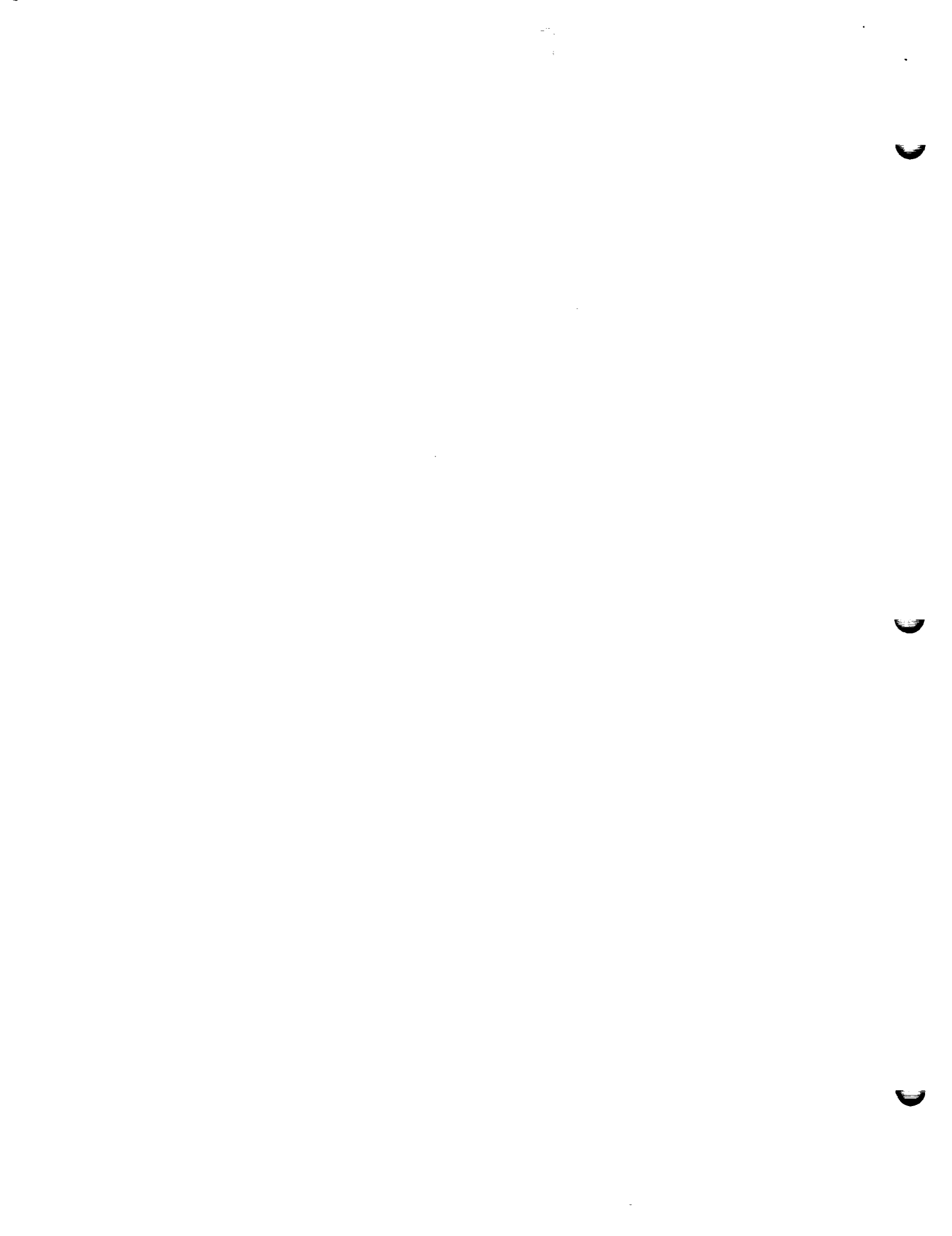
TARGET FRAGMENTS IN COLLISIONS OF 1.8 GeV/NUCLEON ^{56}Fe NUCLEI WITH PHOTOEMULSION NUCLEI, AND THE CASCADE-EVAPORATION MODEL

V.E. DUDKIN, E.E. KOVALEV and N.A. NEFEDOV

Institute of Biomedical Problems of the Ministry of Public Health of the USSR, Moscow, 123007, USSR

V.A. ANTONCHIK, S.D. BOGDANOV and V.I. OSTROUMOV

Leningrad Polytechnical Institute, Leningrad, USSR

E.V. BENTON

University of San Francisco*, San Francisco, CA 94117, USA

H.J. CRAWFORD

Space Science Laboratory, University of California, Berkeley, CA 94720, USA

Abstract: Nuclear photographic emulsion is used to study the dependence of the characteristics of target-nucleus fragments on the masses and impact parameters of interacting nuclei. The data obtained are compared in all details with the calculation results made in terms of the Dubna version of the cascade-evaporation model (DCM).

E | NUCLEAR REACTIONS Target-nucleus, photoemulsion method, cascade-evaporation model, fragmentation, relativistic nuclear collisions.

---

1. Introduction

Successful acceleration of relativistic heavy-ion beams up to iron has provided researchers with auspicious possibilities for studying the features of high-energy nuclear interactions. In this connection, any information on non-relativistic secondaries (the upper boundary of their energy spectrum is ususally taken to be 400 MeV/nucleon), whose characteristics are defined mainly by processes in the target nuclei [1]), proves to be of great importance when constructing and verifying any models which would be adequate to explain experimental data.

109

The characteristics of non-relativistic secondaries in reactions of relativistic nuclei p, ^{12}C, ^{16}O, and ^{22}Ne were studied in detail in previous works [2-4]), where comprehensive comparison with calculation results obtained in terms of the cascade-evaporation model was used to conclude that the given model is qualitatively applicable to describing the characteristics of singly-charged particles emitted from emulsion nuclei. It is of interest, therefore, to study the characteristics of target–nucleus fragments in the collisions initiated by a much heavier projectile nucleus.

2. Experiment

The present work continues the studies of collisions of 1.8 GeV/nucleon ^{56}Fe nuclei with emulsion nuclei [5-8]). The experimental conditions, the search methods and the initial processing of the events were described earlier [8]). The secondaries with energies below 400 MeV/nucleon were charge- and energy-separated by the same techniques as in refs. [2-4]). All singly-charged particles were assumed to be protons, while all doubly-charged particles were regarded as α-particles.

The experimental statistics amounted to 558 events. In conformity with Dudkin et al. [8]), the studied events were classified into interactions of Fe nuclei with the light (CNO) and heavy (AgBr) nuclei of photoemulsion. A class of interactions was also singled out in which the number of h particles, i.e. particles with energies below 400 MeV/nucleon, exceeded 27. The given events occur as a result of almost complete breakup of target nuclei.

The calculations were made in terms of the Dubna version of the cascade model (DCM) [9-11]). The calculation statistics amounted to 4767 events. All the model-calculated interactions were recorded on magnetic media and were then processed using the same criteria as those applied to the real events.

3. Analysis

Following refs. [2-4]), the energy range of secondaries was divided in our analysis into two sub-ranges: fast particles ($30 < E_p < 400$ MeV, $40 < E_\alpha < 1600$ MeV) and slow particles ($E_p \leq 30$ MeV, $E_\alpha \leq 40$ MeV).

Tables 1 and 2 present the mean values of multiplicities $\langle n \rangle$, emission angles $\langle \Theta \rangle$, energies $\langle E \rangle$, transverse $\langle p_\perp \rangle$ and longitudinal $\langle p_\parallel \rangle$ momenta (or "forward/backward" (f/b) ratio) obtained in our experiment for protons and α-particles with energies below 400 MeV/nucleon. The DCM calculation results are presented in brackets.

Figs. 1 and 2 show the experimental and calculated energy spectra of protons and α-particles from the Fe+CNO and Fe+AgBr interactions, and from the collisions accompanied by almost complete breakup of a heavy target nucleus ($n_h \geq 28$).

From table 1 it is seen that the mean multiplicity of fast protons ($E > 30$ MeV) increases with increasing target–nucleus mass or with decreasing impact parameters

TABLE 1

Characteristics of 30–400 MeV protons and 10–400 MeV/n α-particles produced in interactions of Fe nuclei ($E_0 = 1.8$ GeV/nucleon) with photoemulsion nuclei (DCM results shown in parentheses)

Interaction type	Secondary-particle species	⟨n⟩	⟨Θ⟩ (degree)	⟨E⟩ (MeV)	⟨P⊥⟩ (MeV/c)	⟨P∥⟩ (MeV/c)
Fe + CNO	p	2.46 ± 0.13 (3.58 ± 0.04)	48 ± 1 (54.3 ± 0.4)	198 ± 5 (166 ± 2)	359 ± 8 (352 ± 3)	394 ± 14 (314 ± 5)
Fe + AgBr	p	11.4 ± 0.3 (13.9 ± 0.1)	52.8 ± 1 (58.9 ± 0.9)	179 ± 3 (161 ± 1)	355 ± 5 (359 ± 1)	345 ± 9 (258 ± 4)
Fe + AgBr ($n_h \geqslant 28$)	p	23.8 ± 0.9 (28.8 ± 0.4)	54 ± 1 (59.0 ± 0.4)	176 ± 4 (162 ± 1)	364 ± 7 (359 ± 2)	338 ± 12 (246 ± 4)
Fe + AgBr	α	0.5 ± 0.1 (0.8 ± 0.1)	58 ± 4 (50 ± 1)	172 ± 24 (273 ± 11)	708 ± 42 (840 ± 20)	373 ± 60 (860 ± 25)
Fe + AgBr ($n_h \geqslant 28$)	α	1.1 ± 0.2 (1.7 ± 0.1)	60 ± 5 (45 ± 1)	186 ± 30 (312 ± 16)	793 ± 74 (885 ± 28)	408 ± 80 (969 ± 35)

TABLE 2

The characteristics of slow protons ($E_p \leqslant 30$ MeV) and α-particles ($E_\alpha \leqslant 40$ MeV) produced in the interactions of 1.8 GeV/nucleon Fe nuclei with photoemulsion nuclei

Interaction type	Secondary-particle energy (MeV)	⟨n⟩ particle/inter-action	⟨Θ⟩ (degree)	⟨E⟩ (MeV)	⟨P_⟩ (MeV/c)	n̄/n̄ [a])
Fe + CNO	$E_p \leqslant 30$	1.66 ± 0.10 (1.45 ± 0.03)	84 ± 2 (83 ± 1)	9.1 ± 0.4 (13.9 ± 0.1)	91 ± 3 (114 ± 2)	1.3 ± 0.2 (1.35 ± 0.04)
Fe + AgBr		5.1 ± 0.2 (6.6 ± 0.1)	86 ± 1 (81.9 ± 0.3)	11.8 ± 0.3 (14.6 ± 0.1)	113 ± 2 (125 ± 1)	1.2 ± 0.1 (1.51 ± 0.04)
Fe + AgBr ($n_h \geqslant 28$)		7.8 ± 0.5 (9.7 ± 0.2)	86 ± 1 (79.1 ± 0.6)	13.3 ± 0.5 (15.8 ± 0.2)	120 ± 3 (130 ± 1)	1.41 ± 0.10 (1.68 ± 0.07)
Fe + CNO	$E_\alpha \leqslant 40$	0.18 ± 0.03 (0.24 ± 0.02)	79 ± 6 (84 ± 1)	17.2 ± 1.2 (14.5 ± 0.6)	264 ± 19 (244 ± 4)	2.2 ± 0.5 (1.30 ± 0.06)
Fe + AgBr		1.1 ± 0.1 (0.4 ± 0.1)	85 ± 3 (85 ± 1)	17.4 ± 0.8 (20.2 ± 0.2)	272 ± 10 (288 ± 2)	1.3 ± 0.2 (1.49 ± 0.07)
Fe + AgBr ($n_h \geqslant 28$)		1.4 ± 0.2 (0.40 ± 0.04)	95 ± 6 (70 ± 1)	20.1 ± 1.2 (18.8 ± 0.3)	286 ± 18 (263 ± 5)	1.0 ± 0.2 (2.91 ± 0.06)

[a]) The ratio of particle emissions to the forward and backward hemispheres.
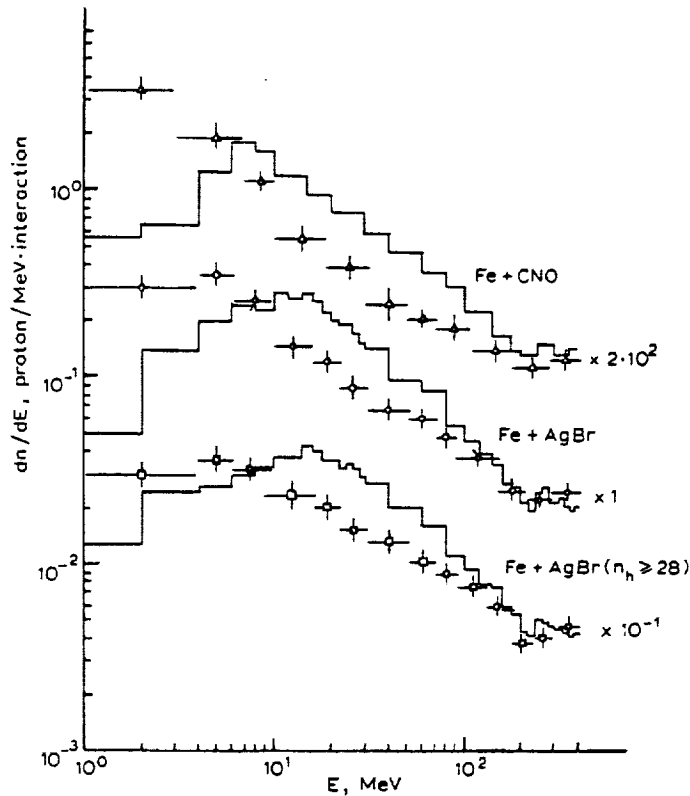
Fig. 1. The $E_p \leqslant 400$ MeV proton energy spectra. Triangles are for Fe + CNO interactions, circles are for Fe + AgBr interactions, and squares are for Fe + AgBr ($n_h \geqslant 28$) interactions. The histograms are the DCM calculation results for these interactions. All data are given in absolute units.

(under transition to the $n_h \geqslant 28$ events). The DCM does describe the increase, but the experimental values prove to be overestimated systematically by 20-30%. At the same time, the calculated mean values of the energies and longitudinal momenta of fast protons prove to be below their experimental values. The experimental and calculated mean transverse momenta are in fairly good agreement with each other. However, the experimental values of mean emission angles of fast protons prove to be below their calculated values (see table 1), reflecting the above-mentioned $p_{\parallel}$ difference.

From the fast-proton energy spectra displayed in fig. 1 it follows that the main difference between the calculated and experimental distributions occurs in the energy range below 100 MeV. It should be noted that the distributions are presented in absolute units without any normalization. At higher proton energies, the calculated and experimental spectra are in fairly good agreement with each other.

Fig. 3 shows the longitudinal and transverse momentum distributions of fast protons produced in the Fe + AgBr interactions. It is seen that the calculated and
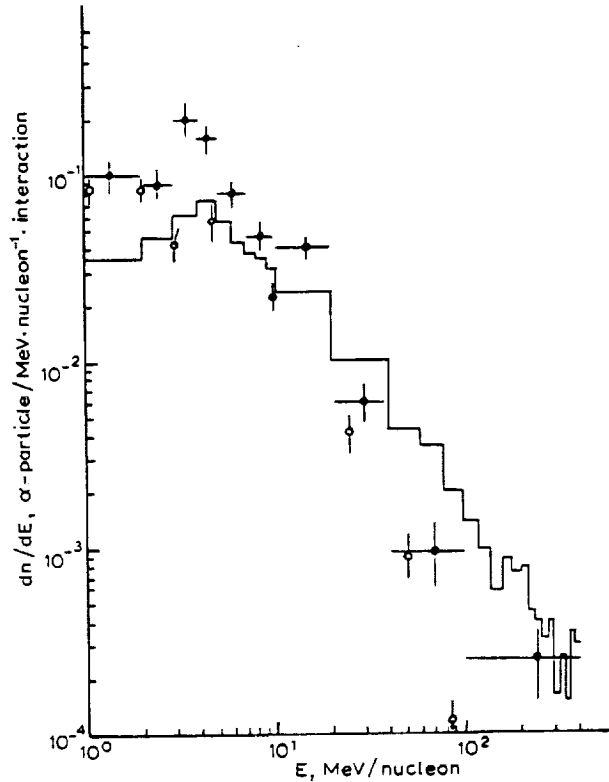
Fig. 2. The $E_a \leqslant 400$ MeV/nucleon α-particle energy spectrum for Fe + AgBr interactions. The points: experiment; the histogram: DCM calculation results.

experimental distributions are in quantitative agreement with each other at the longitudinal and transverse momenta above 400 MeV/c. At lower values of $p_\parallel$ and $p_\perp$, the "model" spectra are 20–30% in excess of the experimental spectra. We are of the opinion that such a systematic overestimation is accounted for by the fact that the calculated 30–100 MeV proton yield is in excess of its experimental value (see fig. 1). Indeed, the momenta of the 30–100 MeV protons are 240–450 MeV/c, so the $p_\parallel$ and $p_\perp$ momentum distributions can get distorted at values below 450 MeV/c. The calculation overestimated 30–100 MeV proton multiplicity in all three interaction classes singled out above, (FE + CNO, Fe + AgBr, and Fe + AgBr ($n_h \geqslant 28$)), gives rise not only to an increase in the total multiplicity of the 30–400 MeV particles, but also to a systematic underestimation of the mean energies and longitudinal momenta of fast protons and to higher values of the mean emission angle (see table 1). Despite the quantitative disagreement, the DCM gives a correct qualitative description of the increase in $\langle \Theta \rangle$ of $E_p > 30$ MeV protons and the decrease in $\langle E \rangle$ and $\langle p_\parallel \rangle$ of the same protons when going from Fe + CNO to Fe + AgBr and to Fe + AgBr ($n_h \geqslant 28$) interactions.

113 *A*
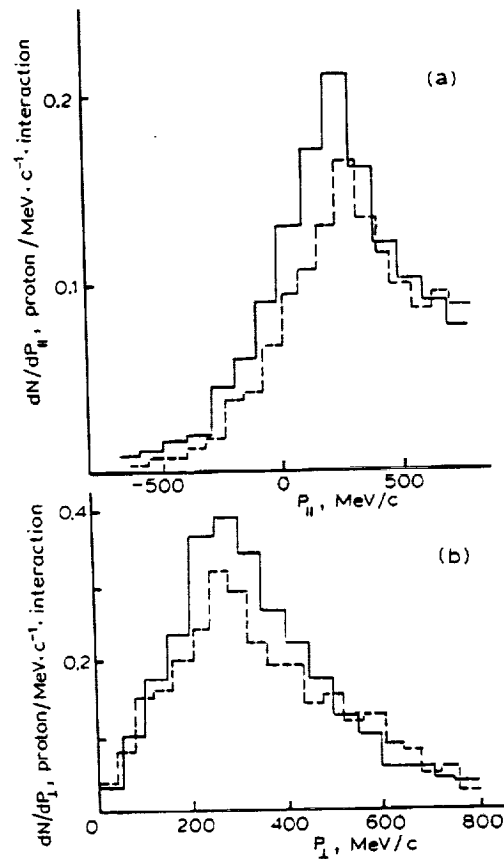
Fig. 3. The longitudinal (lab) (a) and transverse (b) momentum distributions of 30–400 MeV protons in the Fe+AgBr interactions. The dashed and solid-line histograms are the experimental and DCM calculation results, respectively.

Discrepancies between the experimental and calculated characteristics of fast α-particles are much larger than for protons. From the energy distributions displayed in fig. 2, it follows that the calculated yields of α-particles with energy more than 80 MeV (20 MeV/nucleon) are much in excess of the experimental values (see table 1). A substantial preference of the model-simulated α-particles for emission in the forward hemisphere (lower values of $\langle \Theta \rangle$) is also worth noting. The above-mentioned differences in mean characteristics and in the energy spectra suggest that the model does not describe the emission of fast doubly-charged particles satisfactorily.

Let us now examine the degree of agreement between experimental and DCM-calculated characteristics of slow singly- and doubly-charged fragments of a target nucleus. From comparing the data presented in table 2 it is seen that the calculated mean proton multiplicity for the Fe + AgBr collisions has been overestimated, and the mean α-particle value underestimated. The calculated mean proton and α-

113^{β}.

particle energies are somewhat in excess of the experimental values for the interactions with both light and heavy emulsion components. The energy spectra of protons and α-particles in the Fe + CNO, Fe + AgBr, and Fe + AgBr $(n_h \geq 28)$ interactions (see figs. 1 and 2) and proton energy spectra $(E_p \leq 30 \text{ MeV})$, for emission angles $\Theta \leq 90°$ and $\Theta > 90°$ (see fig. 4a, b), indicate a small number of the "sub-barrier" fragments of a target nucleus $(E_p < 4 \text{ MeV})$ in model-simulated interactions compared with experimental data. The given differences in the forms of the experimental and calculated spectra are observed in both forward and backward hemispheres (see fig. 4a, b).

The calculated transverse momenta are higher than their experimental values not only in the "mean" interactions but also in the subset of Fe + AgBr $(n_h \geq 28)$ (see table 2), thereby indicating that the model temperature of the excited residual target-nucleus is, on the average, higher than its experimental value. A higher excitation of target nucleus leads to a higher number of evaporated protons and to a lower multiplicity of low-energy α-particles (the relative probability for doubly-charged particles to be emitted decreases sharply at high excitation energies in the evaporation model). This assertion was verified by comparing the measured and
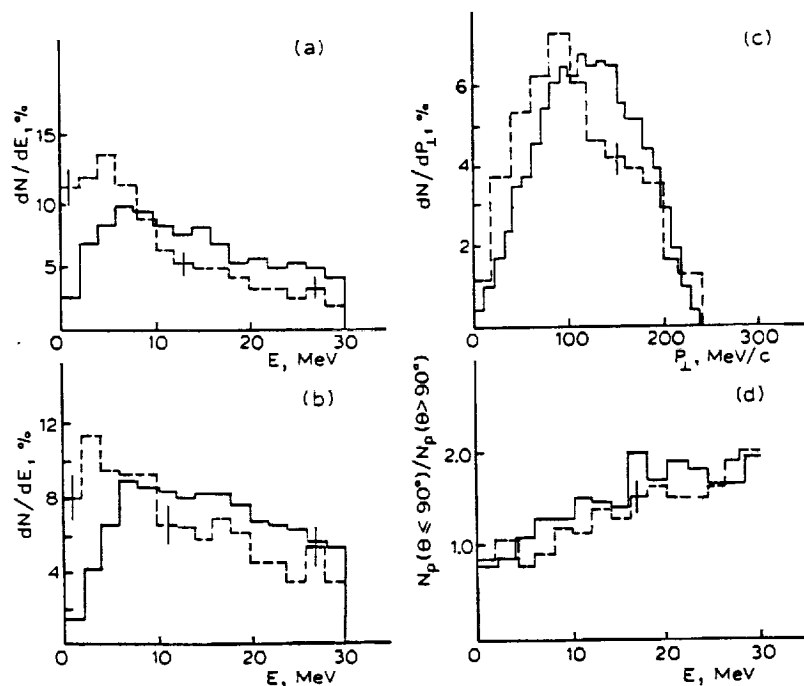
Fig. 4. The characteristics of $E_p \leq 30$ MeV protons in the Fe + AgBr interactions: the energy spectra at forward (a) and backward (b) hemispheres; the transverse-momentum distribution (c), and the "forward-to-backward" ratio energy dependence (d), the dashed and solid-line histograms are the experimental and DCM calculation results, respectively.

113^c

calculated transverse-momentum $(p_\perp)$ distributions of the $E \leqslant 30$ MeV protons in AgBr interactions (see fig. 4c). It is seen that the calculated and experimental distributions are shifted with respect to each other but display the same form. The "effective" temperature of the particle-emitting system may be estimated assuming that the singly-charged particle distribution of each of the 3-momentum components corresponds to a gaussian distribution with parameter $\sigma = \sqrt{2/\pi}\langle P_\perp \rangle$ and that the "effective" temperature is: $T_0 = \sigma^2/m$. The estimate inferred in such a manner from experimental data is $T_0 \sim 7$ MeV, whereas the model-calculated "effective" temperature proves to be about 10 MeV.

Examination of the angular distributions (not presented here) and of the mean emission angles of low energy protons and α-particles (see table 2) has shown that the experimental distributions exhibit a smaller forward asymmetry compared with the model. The calculated f/b ratios for all interactions (1.51 ± 0.14) and for the "central" interactions at $n_h \geqslant 28$ (1.68 ± 0.07) are markedly in excess of their experimental values, 1.2 ± 0.1 and 1.4 ± 0.1, respectively. The disagreement is preserved also in the f/b energy dependence (fig. 4d), although the character of its behavior (an increase of anisotropy with increasing energy) is represented correctly by the model.

Thus, the consistent comparison between the experimental and DCM-calculated characteristics of fast and slow fragments of a target nucleus has shown that higher numbers of both nucleons and complex particles are emitted from target-nuclei during the first (fast) interaction stage in the DCM-simulated events compared with experimental data. As a result, at the end of the cascade, the "model" residual target nuclei have a higher "effective" temperature T_0 and a higher longitudinal velocity $\beta_\parallel$. The resultant anomalously-high T and $\beta_\parallel$ give rise to an increased mean energy of the particles emitted from residual nuclei. Therefore, the number of the $E \leqslant 5$ MeV particles in the model interactions (even with light nuclei) is significantly decreased.

The effect of the projectile mass on the low-energy particle characteristics ($E_p \leqslant$ 30 MeV, $E_\alpha \leqslant 40$ MeV) was studied in the present work by comparing the results obtained with the earlier experimental data [2,4,12]). With this purpose, following Antonchik et al. [12]), we plotted the distributions of longitudinal velocity $\beta_\parallel$ of emitted particles (see fig. 5) and approximated the plots by the gaussian distributions:

$$\frac{\mathrm{d}N}{\mathrm{d}\beta_\parallel} \sim \exp\left[-\frac{(\beta_\parallel - \langle\beta_\parallel\rangle)^2}{\beta_0^2} \right] \tag{1}$$

where β_0 is the characteristic velocity of the particles emitted from an excited nucleon system; $\langle\beta_\parallel\rangle$ is the mean longitudinal velocity of the system.

In this case [12]), the "effective" temperature T_0 of the particle-emitting system is $T_0 = \frac{1}{2}m\beta_0^2$, where m is an emitted particle mass.

The longitudinal velocity distributions of the $E \leqslant 30$ MeV proton and of the $E \leqslant 40$ MeV α-particles, shown in fig. 5 are quite properly approximated by gaussian distributions [1]) in agreement with the assumption that residual target-nuclei can be

113^b
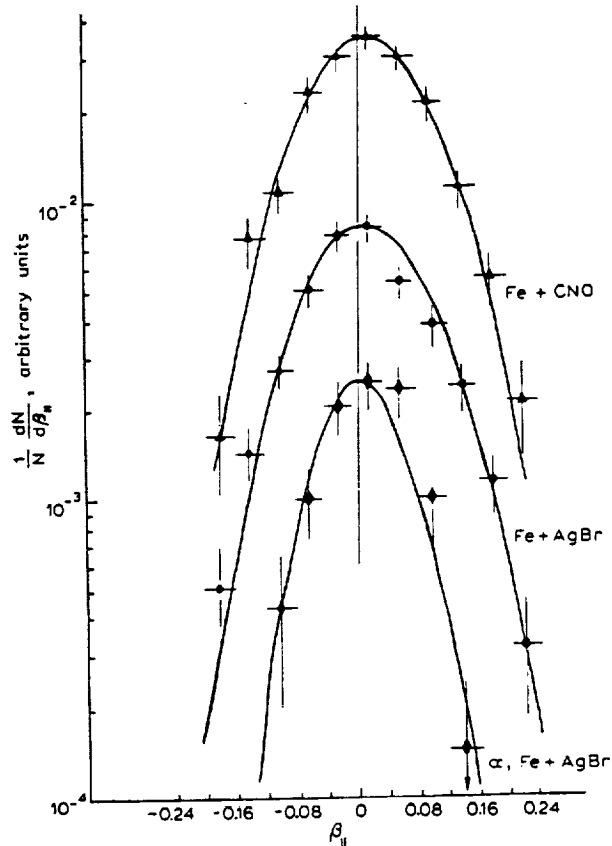
Fig. 5. The longitudinal (lab) velocity $(\beta_\parallel)$ distributions for $E_p \leqslant 30$ MeV secondary protons in the Fe+CNO (triangles) and Fe+AgBr (circles) interactions, and for $E_\alpha \leqslant 40$ MeV α-particles in the Fe+AgBr (diamonds) interactions. The curves are the approximations by gaussian distributions.

represented as a distribution of excited nucleon systems moving longitudinally at velocity $\langle \beta_\parallel \rangle$ and emitting particles isotropically.

Table 3 presents the $\langle \beta_\parallel \rangle$ and $\langle \beta_0 \rangle$ values inferred from experimental and model-calculated (in parentheses) data and shows also the results obtained elsewhere. The set of data presented in table 3 indicates that the mean longitudinal velocity of the system is rather low and varies within the $0.005 < \langle \beta_\parallel \rangle < 0.02$ range, irrespective of the projectile mass. At the same time, a systematically-higher velocity of the residue of light target-nuclei is observed.

Analysis of the values of β_0 presented in table 3 shows that β_0 remains in practice constant at a level of 0.10–0.12 as energy increases or the target nucleus changes and when the impact parameter in the collisions with heavy (AgBr) nuclei (transition to $n_h \geqslant 28$ collisions) decreases, thereby indicating that the "effective" temperature T_0, which characterizes the excitation energy of the target nucleus per nucleon [12],

TABLE 3

Characteristics of the excited nucleon system emitting slow particles (DCM results shown in parentheses)

Interaction type	Projectile energy [GeV/nucleon]	Secondary particle	$\langle \beta_\parallel \rangle$	$\langle \beta_0 \rangle$	Ref.
Fe+CNO	1.8	Protons $E_p \leqslant 30$ MeV	0.016 ± 0.005 (0.003 ± 0.002)	0.110 ± 0.010 (0.137 ± 0.003)	this work
Fe+AgBr	1.8		0.011 ± 0.003 (0.019 ± 0.002)	0.118 ± 0.004 (0.150 ± 0.002)	this work
Fe+AgBr $(n \geqslant 28)$	1.8		0.013 ± 0.004 (0.025 ± 0.003)	0.121 ± 0.007 (0.156 ± 0.003)	this work
Ne+CNO	3.6		0.011 ± 0.007	0.110 ± 0.010	[4]
Ne+AgBr	3.6		0.005 ± 0.003	0.125 ± 0.005	[4]
p+CNO	3.6		0.007 ± 0.008	0.120 ± 0.010	[2]
p+AgBr	3.6		0.003 ± 0.003	0.103 ± 0.004	[2]
Fe+AgBr	1.8	α-particles $E_\alpha \leqslant 40$ MeV	0.007 ± 0.004 (0.013 ± 0.002)	0.08 ± 0.01 (0.07 ± 0.01)	this work
Ne+AgBr	3.6		0.009 ± 0.003	0.08 ± 0.02	[4]
p+AgBr	3.6		0.013 ± 0.005	0.08 ± 0.03	[2]
He+AgBr	2.1	$R < 4$ mm $E_p < 31$ MeV	0.016 ± 0.004	0.117 ± 0.002	
O+AgBr	2.1		0.015 ± 0.004	0.115 ± 0.002	[12]
Ar+AgBr	2.1		0.012 ± 0.002	0.117 ± 0.002	

is also constant. The value of T_0 for low-energy protons was estimated to be 5–7 MeV for all of the experimental data presented in table 3. The DCM calculations lead (as mentioned above) to a higher "effective" temperature and to a higher longitudinal velocity of the emitted low-energy particles.

4. Conclusions

The main results of the present work may be summarized as follows:

(1) The energy, momenta, and angle characteristics of singly- and doubly-charged fragments of target nuclei have been obtained for interactions of 1.8 GeV/nucleon ^{56}Fe nuclei with light and heavy nuclei in emulsions; the dependencies of these characteristics on target mass have been studied.

(2) The consistent comparison with the DCM calculation results has shown that the DCM describes the differential energy spectra of protons with energy $E >$ 100 MeV but does not describe the emission of fast complex particles. The high model-simulated excitation energies, which exceed their experimental values, distort the energy spectra of low-energy particles.

114^B

(3) The increase of projectile nucleus mass from proton to iron in the relativistic energy range (1.8-3.6 GeV/nucleon) does not significantly affect the characteristics of an excited nucleon system which emits slow particles. This is consistent with the concept of factorization.

References

1) V.S. Barashenkov and V.D. Toneev, Interaction of high-energy particles and atomic nuclei with nuclei Atomizdat, Moscow (1972)
2) V.A. Antonchik et al., Yad. Fiz. (Sov. J. Nucl. Phys.) 40, no. 3(9) (1984) 752
3) Cosice-Leningrad, collaboration, Yad. Fiz. (Sov. J. Nucl. Phys.) 28 (1978) 435
4) V.A. Antonchik et al., Yad. Fiz. (Sov. J. Nucl. Phys.) 46, no. 5(11) (1987) 1344
5) V.A. Antonchik et al., Yad. Fiz. (Sov. J. Nucl. Phys.) 35, no. 5(11) (1982) 1103
6) V.A. Antonchik et al., Yad. Fiz. (Sov. J. Nucl. Phys.) 42, no. 6(12) (1985) 1289
7) V.A. Antonchik et al., Yad. Fiz. (Sov. J. Nucl. Phys.) 44, no. 6(12) (1986) 1508
8) V.E. Dudkin, E.E. Kovalev, N.A. Nefedov, V.A. Antonchik, S.D. Bogdanov, V.I. Ostroumov, H.J. Crawford and E.V. Benton, Nucl. Phys. A509 (1990) 783
9) K.K. Gudima and V.D. Toneev, Yad. Fiz. (Sov. J. Nucl. Phys.) 27 (1978) 658
10) K.K. Gudima, H. Iwe and V.D. Toneev, J. Phys. G2 (1979) 237
11) K.K. Gudima and V.D. Toneev, Nucl. Phys. A400 (1983) 173
12) H.H. Heckman et al., Phys. Rev. C17 (1978) 1651

114ᶜ